

Supersolid phase of cold atoms[★]

Tie-Fu Zhang^{1,2}, Wei Han^{3,4}, Ren-Yuan Liao^{5,6}, Jin-Wu Ye^{7,8}, and Wu-Ming Liu^{1,2,9,a}

¹ Beijing National Laboratory for Condensed Matter Physics, Institute of Physics, Chinese Academy of Sciences, Beijing 100190, P.R. China

² School of Physical Sciences, University of Chinese Academy of Sciences, Beijing 100049, P.R. China

³ Key Laboratory of Time and Frequency Primary Standards, National Time Service Center, Chinese Academy of Sciences, Xi'an 710600, P.R. China

⁴ School of Astronomy and Space Science, University of Chinese Academy of Sciences, Beijing 100049, P.R. China

⁵ Fujian Provincial Key Laboratory for Quantum Manipulation and New Energy Materials, College of Physics and Energy, Fujian Normal University, Fuzhou 350117, P.R. China

⁶ Fujian Provincial Collaborative Innovation Center for Optoelectronic Semiconductors and Efficient Devices, Xiamen 361005, P.R. China

⁷ Department of Physics and Astronomy, Mississippi State University, Starkville, MS 39762, USA

⁸ Kavli Institute of Theoretical Physics, University of California, Santa Barbara, CA 93106, USA

⁹ Songshan Lake Materials Laboratory, Dongguan, Guangdong 523808, P.R. China

Received 1 March 2020 / Received in final form 6 April 2020

Published online 1 July 2020

© EDP Sciences / Società Italiana di Fisica / Springer-Verlag GmbH Germany, part of Springer Nature, 2020

Abstract. Supersolid phase is a phase of matter that is characterized by the combination of the off-diagonal long-range order of superfluid and the diagonal long-range order of solid. Cold atoms with spin-orbit-coupling, contact interaction and long-range interaction can provide systems for the research of supersolid phase. Under the effect of spin-dependent potential and spin-orbit-coupling, hard-core ultracold atoms with contact interaction can be shown to construct supersolid phase. The combination of soft-core long-range interaction and spin-orbit coupling can establish exotic supersolid phase with spontaneous breakdown of chiral symmetry. The optical Bragg scattering of cold atoms in optical lattices can be used to detect supersolid phase. The study of supersolid phase will be helpful to the researches of matter phases.

1 Introduction

Supersolid phase is a phase of matter that contains the coexistence of the off-diagonal long-range order of superfluid and the diagonal long-range order of solid [1–10]. To get this supersolid phase, the breaking of two continuous symmetries is necessary: continuous translational invariance of crystal and phase invariance of superfluid [1–3].

Since 1969, there is a long history about the searching for supersolid phase [11–16]. Recently, Helium-4 has been considered to construct the experimental observation of supersolid phase [5,7–10]. It is suggested that the existence of supersolid phase can be found in condensates of both hard-core and soft-core bosons with interaction of long-range by theoretical analysis [17–22]. Systems of ultra-cold atoms construct a convenient platform to investigate many kinds of quantum phenomena, because of the high controllability of optical lattices. Various phases of

Bose gases have been observed by the combination among the external potential, interatomic interaction and spin-orbit-coupling. The phenomena of supersolids can also be investigated in the system of ultra-cold atomic gas with spin-orbit-coupling.

Although there are abundant researches of spin-orbit-coupling, many of these studies just concentrate on the system of hard-core, that the interaction between atoms can be considered as zero-range contact. Besides that, too much attention has been attracted on the low dimensional systems, however, on the base of many great studies of one-dimensional and two-dimensional spin-orbit-coupling, supersolid phase in high dimensional systems can be investigated conveniently.

In this article, several circumstances related to inducing and observing supersolid phase are reviewed. Such as the spin-orbit-coupling in hard-core Bose gas with spin-dependent periodic potential which can generate the supersolid phase [1], the soft-core long-range interaction that can establish the chiral supersolid phase [2], the supersolid phase in three-dimensional Bose gas with Rashba type spin-orbit-coupling [3] and optical Bragg scattering in optical lattices to detect supersolid phase [4].

[★] Contribution to the Topical Issue “Topological Ultracold Atoms and Photonic Systems”, edited by G. Juzeliūnas, R. Ma, Y.-J. Lin and T. Calarco.

^a e-mail: wmliu@iphy.ac.cn

It is surprising that the combination of soft-core long-range interaction and spin-orbit-coupling can induce the chiral supersolid with the spontaneous circulating of particles. The chirality imposed by spin-orbit-coupling is considered to generate a finite angular momentum. It is also revealed that different types of spin-orbit-coupling such as Dresselhaus type and Rashba type can induce the opposite chirality of the current of particles.

2 Supersolid induced by spin-orbit-coupling

It is a long history about the search of supersolids; nevertheless, short range interaction on the system of supersolids in hard core bosons is of considerable in recent times.

Under the effect of spin-dependent periodic potential, we focus on two component Bose-Einstein condensates with spin-orbit-coupling. This spin-orbit-coupling is realized by the field of period pulsed potential, that is classified as Rashba-Dresselhaus type [23,24]. In general, the laser beams of counter-propagating cross-polarized type can be used to produce spin-dependent periodic potential [25,26]. By the means of Gross-Pitaevskii mean-field approximation, the Hamiltonian [1] can be represented as:

$$\mathcal{H} = \int d\mathbf{r} \Psi^\dagger \left(-\frac{\hbar^2 \nabla^2}{2m} + \mathcal{V}_{\text{so}} \right) \Psi + \int d\mathbf{r} \sum_{\alpha=\uparrow,\downarrow} V_\alpha \Psi_\alpha^* \Psi_\alpha + \frac{1}{2} \int d\mathbf{r} \sum_{\alpha,\beta=\uparrow,\downarrow} g_{\alpha\beta} \Psi_\alpha^*(\mathbf{r}) \Psi_\beta^*(\mathbf{r}) \Psi_\beta(\mathbf{r}) \Psi_\alpha(\mathbf{r}) \quad (1)$$

where $\Psi = [\Psi_\uparrow(\mathbf{r}), \Psi_\downarrow(\mathbf{r})]^\top$ is the normalized order parameter with complex value, which is normalized by the number of whole particles expressed as $\int d\mathbf{r} \Psi^\dagger \Psi = N$. $a_{\alpha\beta}$ is the s -wave scattering length which characterizes the interaction strength of the atoms $g_{\alpha\beta} = 4\pi\hbar^2 a_{\alpha\beta}/m$. The term of spin-orbit-coupling is defined as $\mathcal{V}_{\text{so}} = -i\hbar(\kappa_x \sigma_x \partial_x + \kappa_y \sigma_y \partial_y)$, where Pauli matrices are described as $\sigma_{x,y}$ and the strengths of spin-orbit-coupling represented as $\kappa_{x,y}$. In the case of $\kappa_x = \kappa_y$ which means isotropic, this type of spin-orbit-coupling is classified as Rashba type. The periodic potentials depend on spin expressed as $V_\uparrow = V_0 \sin^2(\pi x/a)$ and $V_\downarrow = V_0 \cos^2(\pi x/a)$, which represent the spin-up and spin-down atoms, respectively (Fig. 1).

In the case that the interaction of atoms is fixed, the transition from the phase of superfluid to the phase of supersolid is observable, with the increasing strength of Rashba spin-orbit-coupling written as κ . Specially, when the strength of spin-orbit-coupling is weak, the ground states of the alternating spin domains' system, where the atoms with spin-up and spin-down fill the stripes are separated. Although the spin-dependent periodic potential breaks the translational symmetry towards the direction of x , the translational symmetry towards the direction of y is preserved. The y direction's translational symmetry will be broken spontaneously if the spin-orbit-coupling is larger than the critical point. In consequence, we consider the stabilized new phase as the superfluid phase, with the

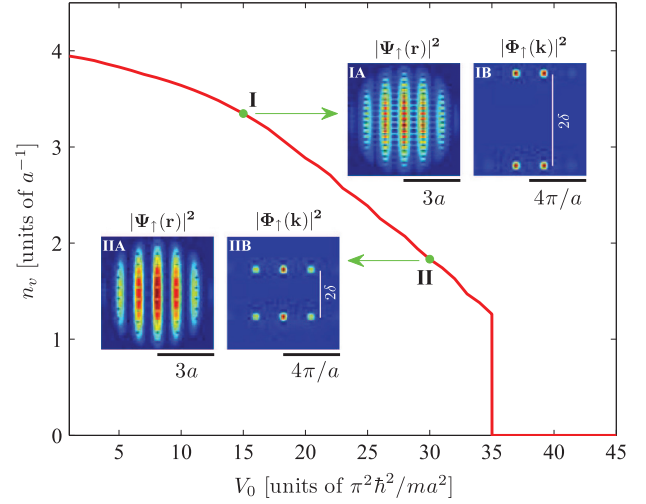


Fig. 1. The line density of vortices as a function of the depth of periodic potential. The line density n_v decreases when the periodic potential depth V_0 increases, and falls to zero when $V_0 = 35\pi^2\hbar^2/ma^2$ which represents the transition point between the phase of supersolid and the phase of superfluid. The insets density change of vortex and the distribution of atomic momentum are described by the insets. The strength of Rashba type spin-orbit-coupling is fixed that $\kappa = 4\pi\hbar/ma$. This figure is taken from reference [1].

periodic density modulation towards y direction. Induced by spin-orbit-coupling, the strip phase towards the direction of y can be used to illustrate this new density modulation. It should be noted that there are some textures of exotica existing with this so called superfluid phase. There are differences between the supersolid phase and the superfluid phase such as the momentum distribution. In the case of superfluid phase, the atoms condensate at discrete points of the edge of the Brillouin zones with finite values of momentum, while in the case of supersolid the peaks of momentum distribution separated from $k_y = 0$ to $k_y = \pm\delta$, where $\delta \in (0, m\kappa/\hbar)$ is the separation distance that depends on the depth of the periodic potential and the strength of the spin-orbit-coupling.

Besides the y direction modulation of density distribution, the chains of vortex and anti-vortex in the domains of spin-up and spin-down construct the vortex lattice that characterize the supersolid phase. The competition of the periodic potential and the spin-orbit-coupling stabilizes these two arrangements of the vortices. In the case of triangular lattice, there are staggered vortices of neighboring chains. While in the case of rectangular lattice, there are parallel vortices of neighboring chains.

It should be noted that there is no direct association between the vortex lattice and the supersolid phase [18], as shown in the system of supersolid droplet crystals. In the traditional systems, artificial magnetic fields and rotation are used to creating supersolid vortices, while the interplay of the interatomic interactions, spin-dependent periodic potential and spin-orbit-coupling can generate vortices directly in the present system [19,22].

The alternating propagating of plane wave on the opposite directions of axis y can be used to illustrate the

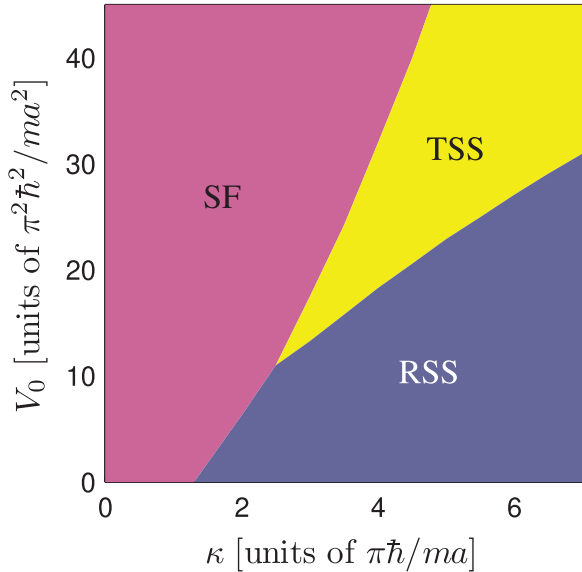


Fig. 2. The diagram of ground-state phase spanned by the Rashba type spin-orbit-coupling strength written as κ and the depth of periodic potential written as V_0 . The phase of superfluid (SF), the phase of triangular supersolid (TSS) and the phase of rectangular supersolid (RSS) can be identified by the phase diagram. The dimensionless parameter of interaction is written as $\tilde{g} = 6000$. This figure is taken from reference [1].

alternating arrangement of the chains of vortex and anti-vortex. If we know that $\oint_C \mathbf{v}_s \cdot d\mathbf{l} = 2\pi\hbar N_v/m$ which is named as Onsager–Feynman quantization condition [27], the vortex line density can be expressed as $n_v = k_y/\pi$, where the wave number is described as $k_y = \delta$. With the increasing of the depth of periodic potential V_0 , the vortex line density decreases to 0 from $m\kappa/\pi\hbar$, in the precondition that there is a given strength of spin-orbit-coupling κ . It is shown in numerical simulations (Fig. 2).

The system of Bose gas with two components can be regarded as the magnetic system. Then there exists the possibility that the transition of the supersolid is related with the ordering of magnetic structure. The vector of spin density is represented as $\mathbf{S} = \Psi^\dagger \boldsymbol{\sigma} \Psi / |\Psi|^2$ with the representation of pseudo-spin, where the vector of Pauli matrix is described as $\boldsymbol{\sigma}$. In the form of meron and anti-meron pair crystal, spontaneous magnetic ordering can be represented by the texture of spin [28]. Meron pairs exist in the domain of spin-up, while anti-meron pairs exist in the domain of spin-down. It should be noted that the topological configuration with the spin-up or spin-down points that rotate away from the core of meron represents the meron. There is a so-called circular hyperbolic structure corresponding to the meron pair of the anti-meron pair with the opposite orientation of spin.

The topological charge (Chern number) Q represented as the spatial integral of the density of topological charge $q(\mathbf{r}) = (1/8\pi) \epsilon^{ij} \mathbf{S} \cdot \partial_i \mathbf{S} \times \partial_j \mathbf{S}$, characterizes the topological spin textures. The density distribution of the topological charge in the cases of rectangular lattice and triangular lattice is presented in the figures. In should be noted that both the pairs of meron and anti-meron are topologically

non-trivial. The value of the topological charge is 1 in the case of meron pair, while the values of the topological charge is -1 in the case of anti-meron pair. In the superfluid phase of topological trivial, the values of the topological charge are 0.

The bulk rotation usually stabilizes the lattices of topological spin texture, such as skyrmion lattices and meron pair [29–31]. In recent times, interplay between harmonic trap and spin-orbit-coupling is used to realize the skyrmion lattices [32]. It is easy to show that the interplay between the spin-dependent periodic potential and the spin-orbit-coupling can also stabilize the skyrmion lattices within a very large regime of the strength of the interaction of atoms. In the conditions of realistic without the method of Feshbach resonance, this strength of interaction can be experimentally realized naturally. Consequently, the method of creating and manipulating the texture of topological spin in the system of spin-orbit-coupling is provided by the above observation.

The supersolid phase properties have been discussed in the sections above and now we can focus on the appearing of superfluid phase when the strength of spin-orbit-coupling is weak. In this case, along the axis y the translational symmetry is preserved, the density modulation of the system is not supported. Nevertheless, the existence of spin-orbit-coupling can break the symmetry of spin-rotation in the plane of S_x – S_y and realize the domain walls of spontaneous chiral.

To illustrate this phenomenon clearly, the effect of spin-orbit-coupling with the two component condensates relative phase $\theta_\uparrow - \theta_\downarrow$, where the phases of the wave functions of spin-up and spin-down are represented as θ_\uparrow and θ_\downarrow , respectively. The Hamiltonian of the system is not dependent on the two components' relative phase when the spin-orbit-coupling is absent. Under the effect of spin-orbit-coupling, except the periodic jumps along the axis x , the phase of superfluid does not alter, then we can get that $\nabla\theta_\uparrow = \nabla\theta_\downarrow = 0$. Because of the translational symmetry, we can make an approximation about the gradient that $\partial_y |\Psi_\uparrow|^2 \simeq \partial_y |\Psi_\downarrow|^2 \simeq 0$, then we can represent the term of spin-orbit-coupling as:

$$\int \Psi^\dagger \mathcal{V}_{\text{so}} \Psi d\mathbf{r} = 2\kappa \int |\Psi_\downarrow| \partial_x |\Psi_\uparrow| \sin(\theta_\uparrow - \theta_\downarrow) d\mathbf{r} \quad (2)$$

the Hamiltonian is dependent with the relative phase written as $\theta_\uparrow - \theta_\downarrow$, under the effective of the spin-orbit-coupling. Let the energy functional minimized, relative phase of the wave function of the ground state is located at the points $\pm\pi/2$, where the sign \pm of this point is corresponding to the sign of the gradient $\partial_x |\Psi_\uparrow|$. Consequently, the modulation of the periodic density along the axis x generates the alternating of a relative phase between the $-\pi/2$ and the $\pi/2$.

The domains of spin-up and spin-down are separated by the domain wall, the type of the domain walls are determined by the relative phase [33]. Analyze the vector of the spin density \mathbf{S} , it is easy to find that the relative density determines the S_z component, while the relative phase determines the spin projection direction in S_y – S_z plane that illustrated by the azimuthal angle $\alpha = \theta_\downarrow - \theta_\uparrow =$

$\arctan(S_y/S_x)$. Without the effect of spin-orbit-coupling, the arbitrary relative phase is found in the two component condensates, then the projection of the spin can have arbitrary direction on the plane S_x - S_y within the domain wall. With the effect of spin-orbit-coupling, the value of the relative phase is $\pm\pi/2$, then the symmetry of spin rotation in the plane S_x - S_y becomes broken. According to the relation that $S_x = 2|\Psi_\uparrow||\Psi_\downarrow|\cos(\theta_\uparrow - \theta_\downarrow) / (|\Psi_\uparrow|^2 + |\Psi_\downarrow|^2)$, in this case we can have $S_x = 0$. Then the spins of the domain wall become restricted in the plane S_y - S_z and the Bloch wall is formed.

One of the domain wall's important properties is the chirality, that characterizes the left-handed rotation from the right-hand rotation. In recent times, the chirality of the domain wall has been explored in the system of ultra-thin ferromagnetic films [34–36]. Opportunities for the design of the spintronics device and the application in the processing of information are given by the chirality of the domain wall. By the means of altering the sign of spin-orbit-coupling of Rashba type, we can manipulate the chirality of Bloch wall in present system. While in the system of real experiment, modulation of the rf field's phase is supposed to alter the sign of the spin-orbit-coupling of Rashba type [23].

Interaction of the symmetry of SU(2) is discussed with the relation that $g_{\uparrow\uparrow} = g_{\downarrow\downarrow} = g_{\uparrow\downarrow}$. More than this situation, the case of $g_{\uparrow\uparrow} = g_{\downarrow\downarrow} \neq g_{\uparrow\downarrow}$ which represents the interaction of the symmetry of non-SU(2) should be considered. It is found that when the phase of the supersolid stabilized with the interplay of the periodical potential depth V_0 with the interaction of SU(2) symmetry and the strength of spin-orbit-coupling κ , the phase of supersolid is favored by the interaction of asymmetry with $g_{\uparrow\uparrow} > g_{\uparrow\downarrow}$. In the case that $g_{\uparrow\uparrow} < g_{\uparrow\downarrow}$, the difference between $g_{\uparrow\downarrow}$ and $g_{\uparrow\uparrow}$ is much smaller than $g_{\uparrow\downarrow}$ that $g_{\uparrow\downarrow} - g_{\uparrow\uparrow} \ll g_{\uparrow\downarrow}$, the phase of the supersolid is stable too. In the case that $g_{\uparrow\uparrow} \ll g_{\uparrow\downarrow}$, the phase of supersolid is unfavorable, and replaced by the phase of superfluid.

Now we focus on the anisotropy effect of spin-orbit-coupling additionally. The phase of supersolid is found with the decreasing of κ_x , in the case of Rashba spin-orbit-coupling, the phase of supersolid is stable in a given range of $\kappa_x < \kappa_y$. With the increasing of the anisotropy, there is a transition to the phase of superfluid of the system. Specially, in the case that $\kappa_x = 0$, the spin-orbit-coupling is unidirectional, and the phase of supersolid with the texture of non-trivial topological spin vanishes.

The system we discussed in this section is thought to be experimentally realized with the condensates of ^{87}Rb atoms by magnetic states written as $|F = 1, m_F = -1\rangle$ and $|F = 1, m_F = 1\rangle$ in the manifold of the ground state that $F = 1$. The combination of the pair of the laser beams of cross-linear polarized counter-propagating and the magnetic pulse can implement the potential of spin-dependent periodic and the spin-orbit-coupling of Rashba type [23–26]. In the case of typical experiment, consider the system of the harmonic potential with frequencies $\omega_z \approx 2\pi \times 200 \text{ Hz}$ and $\omega_\perp \approx 2\pi \times 40 \text{ Hz}$ that trap the atoms with the number of total atoms $N = 1.7 \times 10^5$

and the scattering length of s -wave $a_{\alpha\beta} \approx 100a_B$ (where a_B describes the Bohr radius), the parameter of effective interaction is obtained that $\tilde{g} \approx 6000$. Using $10.6 \mu\text{m}$ CO₂ laser, the lattice constant a can be produced coinciding with the value $\pi\sqrt{\hbar/m\omega_\perp}$.

By the measurements of momentum distribution using the technique of time-of-flight imaging [37] or the in-situ measurements [38,39] of the structure of lattice, the phase of supersolid can be identified. By the imaging technique of the magnetization-sensitive phase-contrast, the configurations of the topological spin of the textures of the meron-pair can be imaged with a high resolution of spatial non-destructively, as well as the domain walls of chiral. The extracting of the relative phase of the imaging technique of dual state can also determine the chirality of domain wall (Fig. 3).

As a conclusion of this section, in the system of spin-dependent periodic potential, Bose-Einstein condensates with the spin-orbit-coupling are reviewed. It is shown that the combination of the spin-dependent periodic potential and the spin-orbit-coupling results in the appearance of the phase of supersolid, that characterizes the coincidental ordering of magnet with the textures of topological non-trivial spin. The diagram of the phase of the system the changing depth of the periodic potential and the strength of the spin-orbit-coupling, the effects of the anisotropic spin-orbit-coupling and the asymmetric interaction of atoms are reviewed. We also discussed the experimental situations about the realization and the observation of the supersolid phase.

3 Chiral supersolid

In this section, the quantum phase of the ground state of Bose gases with the long-range interactions of soft-core and spin-orbit-coupling is reviewed. It is surprising that the interplay between the long-range interaction of soft-core and spin-orbit-coupling can result in chiral supersolid spontaneous circulation of the particles of which appears in all of the unit cells [2]. Then the chirality under the effect of the spin-orbit-coupling generates an angular momentum of finite value [40,41], which violates the general prediction that the many-body system's ground states can not have the total angular momentum with finite value and goes further than the conventional means of the angular momentum yielded by the synthetic magnetic fields [42] or the external rotation [43,44]. The angular momentum's orientation is corresponding to the separation form of the phase, able to be changed by the adjusting of the inter-atom interaction or the strength of spin-orbit-coupling. It should be noted that the different type of the spin-orbit-coupling such as Rashba type or Dresselhaus type results in opposite orientation of particle current chirality.

Consider the system of Bose-Einstein condensate with the homogeneous two-dimensional spin-orbit-coupling and the long-range interaction of soft-core. Using the Gross-Pitaevskii mean-field approximation, Hamiltonian

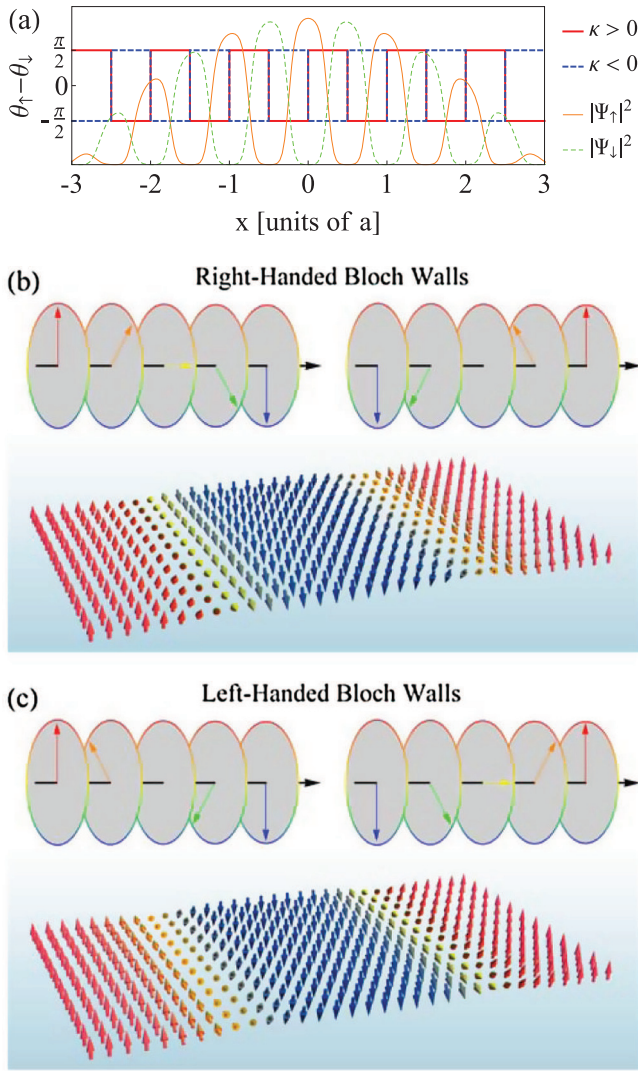


Fig. 3. Chirality of the domain wall. (a) The relative phase section view along axis x , where relative phase is written as $\theta_\uparrow - \theta_\downarrow$. The relative phase is fixed at $\pm\pi/2$ by the effect of Rashba type spin-orbit-coupling, and the relative phase periodic modulation between $\pi/2$ and $-\pi/2$ is induced by the densities' periodic change along axis x . (b) Bloch walls of right-handed chirality stabilized by positive strength of Rashba type spin-orbit-coupling that $\kappa > 0$. (c) Bloch walls of left-handed chirality stabilized by negative strength of Rashba type spin-orbit-coupling that $\kappa < 0$. These figures are taken from reference [1].

of this system is represented as:

$$\begin{aligned} \mathcal{H} = & \int d\mathbf{r} \Psi^\dagger \left(-\frac{\hbar^2 \nabla^2}{2M} + \mathcal{V}_{\text{SO}} \right) \Psi \\ & + \frac{1}{2} \int d\mathbf{r} \sum_{i,j=\uparrow,\downarrow} g_{ij} \Psi_i^*(\mathbf{r}) \Psi_j^*(\mathbf{r}) \Psi_j(\mathbf{r}) \Psi_i(\mathbf{r}) \\ & + \frac{1}{2} \int d\mathbf{r} d\mathbf{r}' \sum_{i,j=\uparrow,\downarrow} \Psi_i^*(\mathbf{r}) \Psi_j^*(\mathbf{r}') U_{ij}(\mathbf{r}-\mathbf{r}') \Psi_j(\mathbf{r}') \Psi_i(\mathbf{r}) \end{aligned} \quad (3)$$

where $\Psi = [\Psi_\uparrow(\mathbf{r}), \Psi_\downarrow(\mathbf{r})]^\top$ is the order parameter of spinor, $\mathbf{r} = (x, y)$ is normalized with $\int d\mathbf{r} \Psi^\dagger \Psi = N$. The term of spin-orbit-coupling is represented as $\mathcal{V}_{\text{SO}} = -i\hbar\kappa(\sigma_x \partial_x \pm \sigma_y \partial_y)$, where Pauli matrices are described as $\sigma_{x,y}$, the strength of spin-orbit-coupling is described as κ . The type of the spin-orbit-coupling is distinguished by the sign \pm , the Rashba type described by sign $+$ while the Dresselhaus type described by sign $-$. The g_{ij} represents the contact interaction strength, in the case of SU(2) symmetry we have $g = g_{\uparrow\uparrow} = g_{\downarrow\downarrow} = g_{\uparrow\downarrow}$. The long-range interaction of the soft-core described by the effective potential which presented as $U_{ij}(\mathbf{r}) = \tilde{C}_6^{(ij)} / (R_c^6 + |\mathbf{r}|^6)$, the interaction strength written as $\tilde{C}_6^{(ij)}$ and the blockade radius written as R_c [45].

The ground states of many-body system can be obtained through the numerically minimizing of the Hamiltonian functional. Without the effect of spin-orbit-coupling, the phase of supersolids with the softening of roton-type mode is induced by the long-range interaction of soft-core [45]. Due to the chiral operation $\hat{O} = \hat{K}$, the Hamiltonian of the system is symmetric. The chiral symmetry is broken by the effect of the type of Rashba or Dresselhaus spin-orbit-coupling and the the phase of exotic chiral supersolid with the phase of clockwise or counter-clockwise circulation possessed each unit cell. Then the two components of spin are separated along the orientation of radius in unit cell. The intra-component interaction always exists in the centre that is surrounded by the stronger intra-component interaction with opposite spin. While the core component's phase is trivial, the vortex of each unit cell is formed by the phase gradient valued 2π along the path closed around the toroidal component. It should be noted that there is a surprising observation that the same orientation of circulation is chosen by all of the vortices, that is distinctive compared to the hard-core system of spin-orbit-coupling, where there are paired vortices and anti-vortices [32,46–51] (Fig. 4).

In order to illustrate the aligned vortices with a better picture, using polar coordinates, the term of Rashba spin-orbit-coupling is written as:

$$\mathcal{H}_{\text{SO}} = -2\kappa \int_{\Lambda_0} d\mathbf{r} \text{Re} \left[\Psi_\uparrow^* \exp(-i\varphi) \left(i \frac{\partial}{\partial r} + \frac{\partial}{r \partial \varphi} \right) \Psi_\downarrow \right] \quad (4)$$

where we write the core component as θ_\bullet , to avoid the dissipation of energy, there must have $\partial \theta_\bullet / \partial \varphi = 0$. Neglect the radial diffusion and consider rotational symmetry, assume that $\partial \theta_j / \partial r = 0$ and $\partial n_j / \partial \varphi = 0$, the term of spin-orbit-coupling becomes:

$$\mathcal{H}_{\text{SO}} = 2\kappa \int_{\Lambda_0} d\mathbf{r} [\sin(\theta_\bullet - \theta_\circ \pm \varphi) \sqrt{n_\circ} \partial_r \sqrt{n_\bullet}] \quad (5)$$

where the component of surrounding toroidal is written as θ_\circ , when the core component is spin-up or spin-down, the sign \pm takes $+$ or $-$. To minimize the energy of spin-orbit-coupling, we have:

$$\theta_\bullet - \theta_\circ \pm \varphi = \frac{\pi}{2} + 2\pi l, \quad (l \in Z) \quad (6)$$

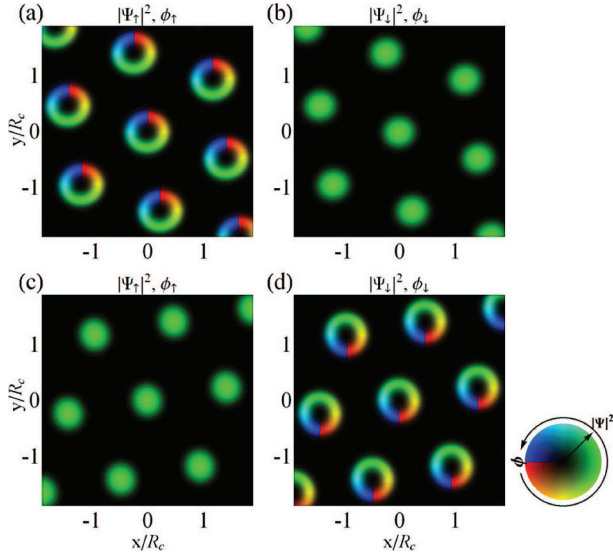


Fig. 4. Chiral supersolid phase induced by soft-core long-range interactions and Rashba type spin-orbit-coupling. The distributions of density and phase are shown in (a) and (b) with the soft-core long-range interactions that $\tilde{C}_6^{(\uparrow\uparrow)}N = 2\tilde{C}_6^{(\downarrow\downarrow)}N = 2500\hbar^2 R_c^4/M$, and in (c) and (d) with the soft-core long-range interactions that $2\tilde{C}_6^{(\uparrow\uparrow)}N = \tilde{C}_6^{(\downarrow\downarrow)}N = 2500\hbar^2 R_c^4/M$. The elevation of quantity is illustrated by the arrow orientation in color wheel. These figures are taken from reference [2].

where the value of the core component θ_\bullet is a constant. Consequently we have the result that the surrounding component θ_\circ tends to have the 2π or -2π valued phase gradient when there is a spin-up or spin-down core component.

The phase non-trivial circulation and the separation of radial phase are considered as the textures of topological spin. Write the Bloch vector as $\mathbf{s} = \Psi^\dagger \sigma \Psi / |\Psi|^2$, project the state Ψ on the unit Bloch surface, we can get that $s_x = \pm\sqrt{1-s_z^2}\sin\varphi$, $s_y = \mp\sqrt{1-s_z^2}\cos\varphi$, and $s_z = (n_\uparrow - n_\downarrow) / (n_\uparrow + n_\downarrow)$.

Within the unit cell, the particle current of spontaneous circulating is acquired by the chiral supersolid. In the theory of hydrodynamic, the conservation of mass requires the presentation of actual particle current with the existence of gauge potential that:

$$\mathbf{j} = \frac{\hbar}{2Mi} [\Psi^\dagger \nabla \Psi - (\nabla \Psi^\dagger) \Psi] - \frac{1}{M} \Psi^\dagger \mathbf{A} \Psi \quad (7)$$

where $\mathbf{A} = -\kappa M (\sigma_x, \sigma_y)$ describes the gauge potential in the case of Rashba type spin-orbit-coupling, $\mathbf{A} = -\kappa M (\sigma_x, -\sigma_y)$ describes the gauge potential in the case of Dresselhaus type spin-orbit-coupling. The first term is the canonical part of the current of the particle that corresponding to the phase gradient $\nabla\theta_j$, the second term is the gauge part due to the phase difference between core and surrounding component $\theta_\bullet - \theta_\circ$. In the case of Rashba spin-orbit-coupling, we represent the current of particle as:

$$\mathbf{j}_R = \frac{\hbar}{M} \frac{n_\circ}{r} \hat{e}_{\pm\varphi} - 2\kappa \sqrt{n_\uparrow n_\downarrow} \hat{e}_{\pm\varphi} \quad (8)$$

where the sing \pm of $\hat{e}_{\pm\varphi}$ is determined by the spin of the core component, that in the case of spin-up we have $\hat{e}_{+\varphi}$ corresponding to counter-clockwise while in the case of spin-down we have $\hat{e}_{-\varphi}$ corresponding to clockwise. The gauge and canonical parts of the currents of the particle always have the opposite orientation of circulation which guarantee the cost of energy keeps less. Specially, in the case that the strength of spin-orbit-coupling is stronger, the gauge part becomes dominant and the orientation of the circulating and the spin in the core of the vortex satisfy the rule of left-hand. In the case of Dresselhaus spin-orbit-coupling, the current of the particle is represented as:

$$\mathbf{j}_D = -\frac{\hbar}{M} \frac{n_\circ}{r} \hat{e}_{\pm\varphi} + 2\kappa \sqrt{n_\uparrow n_\downarrow} \hat{e}_{\pm\varphi} \quad (9)$$

then the opposite particle current chirality is induced by the spin-orbit-coupling of Dresselhaus type.

It is implied by the existence of the chiral circulating current, that there is an angular momentum of finite value exists in the supersolid phase ground state. In unit cell, the Rashba spin-orbit-coupling induces the angular momentum that represented as:

$$l_z = \pm \int_{\Lambda_0} d\mathbf{r} [\hbar n_\circ - 2\kappa M \sqrt{n_\uparrow n_\downarrow} r] \quad (10)$$

the system's total angular momentum can not be zero, because all the vortices circulate with the same orientation. It should be noted that the breaking of chiral symmetry leads to the appearance of the finite angular momentum. Additionally, the orientation of the spin in the core of vortex determines the angular momentum's direction. Therefore, the changing of the relative strength of the interactions of the intra-component expressed as $\tilde{C}_6^{(\downarrow\downarrow)}$ and $\tilde{C}_6^{(\uparrow\uparrow)}$ can alter the direction of angular momentum.

In chiral supersolid, the angular momentum of total spin is non-zero too. Through the numerical simulations, it is found that there are much more particles in the core of vortex with weak strength of intra-component interaction, than the particles in surrounding ring. As the parameters are examined, the surrounding component just constitutes less than 10% particles in total. It is also found that the orientations of the orbital angular momentum and the total spin angular momentum are same in the case of Dresselhaus spin-orbit-coupling while opposite in the case of Rashba spin-orbit-coupling.

The phase diagram of the ground state is considered as the function of the strengths of spin-orbit-coupling and the long-range interaction of soft-core by the means of running the codes of parameter grid values. We have discussed the phase of chiral supersolid (CSS) before, and discover other two types of supersolid phase that are named as the phase of standing-wave supersolid (SWSS) and the phase of plane-wave supersolid (PWSS). The system renders a breaking of translational symmetry to construct the structure of crystalline, as the demand of the phase of supersolid in both SWSS and PWSS cases. In the case of SWSS phase, the strip formation and modulation of density characterize the wave function of condensate. In the

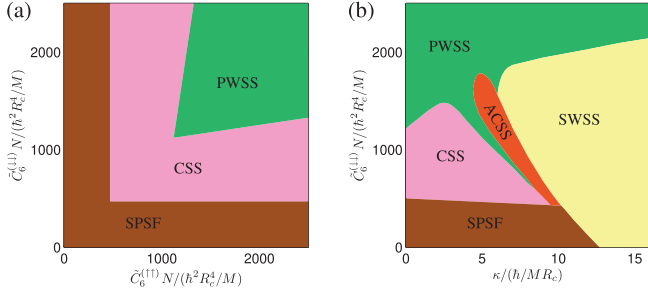


Fig. 5. (a) Phase diagram generated by changing the strengths of soft-core long-range interaction written as $\tilde{C}_6^{(1\downarrow)}$ and $\tilde{C}_6^{(1\uparrow)}$. The strength of spin-orbit-coupling is fixed that $\kappa = 4\hbar/MR_c$. (b) Phase diagram generated by changing the strength of Rashba type spin-orbit-coupling written as κ and the strength of soft-core long-range interaction written as $\tilde{C}_6^{(1\downarrow)}$. The strength of soft-core long-range interaction is fixed that $\tilde{C}_6^{(1\uparrow)}N = 2500\hbar^2R_c^4/M$. These figures are taken from reference [2].

case of PWSS phase, along the given direction the modulation of phase is featured by the wave function of local condensate in unit cell. It should be noted that the local structures of the phases of SWSS and PWSS are similar to the phases of strip and plane-wave, which is due to competition between the interactions of inter-component and intra-component.

In the case that $\tilde{C}_6^{(1\downarrow)} = \tilde{C}_6^{(1\uparrow)}$, the Hamiltonian of the system possesses a symmetry of time reversal expressed as $\hat{T} = i\sigma_y \hat{K}$. In chiral supersolid ground state, this time reversal symmetry will be broken spontaneously (Fig. 5).

The phase of anomalous chiral supersolid (ACSS) phase is found in the phase diagram. The chirality is featured by the ACSS phase with finite orbital and spin angular momenta as well as the phase of CSS investigated before. There is a difference that weaker intra-component interaction spin component prefers to dwell in surrounding toroidal ring than the core of vortex. In the case of traditional Bose-Einstein condensate without the effect of spin-orbit-coupling, this separation of phase is unfavorable in general [52]. Nevertheless, in the case of strong spin-orbit-coupling, a large angular momentum is required that is accommodated by the higher density of particle number easily. It should be noticed that by the means of adjusting the interatomic interaction and the strength of spin-orbit-coupling, the phases of CSS can be turned to the phases of ACSS through the phase transition, the orientation of the angular momentum can also be changed.

In the case that one of the interactions of intracomponents $\tilde{C}_6^{(1\downarrow)}$ and $\tilde{C}_6^{(1\uparrow)}$ is weak, the existence of the phase of spin-polarized superfluid is found. In this spin-polarized superfluid phase, the component of long-range interaction of soft-core is where all the particles condensate, the phase and the density distribution in space is uniformed.

As the conclusion of this section, with the effect of long-range interaction of soft-core, the phase diagram of the ground state of the Bose gases of spin-orbit-coupling is

reviewed. The supersolid phase with exotic chirality can be stabilized in this system.

4 Supersolid in three-dimensional system

With the effect of in-plane isotropic spin-orbit-coupling of Rashba type, the system of homogeneous three-dimensional two-species Bose gases [3] is considered and represented by the Hamiltonian:

$$H = \int d^3\mathbf{r} \sum_{\sigma=\uparrow,\downarrow} \left[\psi_{\sigma}^{\dagger} \left(-\frac{\hbar^2 \nabla^2}{2m} - \mu \right) \psi_{\sigma} + g (\psi_{\sigma}^{\dagger} \psi_{\sigma})^2 \right] + \int d^3\mathbf{r} \left[2g_{\uparrow\downarrow} \psi_{\uparrow}^{\dagger} \psi_{\uparrow} \psi_{\downarrow}^{\dagger} \psi_{\downarrow} + \left(\psi_{\uparrow}^{\dagger} \hat{R} \psi_{\downarrow} + h.c. \right) \right] \quad (11)$$

where the ψ_{σ} and ψ_{σ}^{\dagger} are bosonic operators which satisfy the relation of commutation that $[\psi_{\sigma}(\mathbf{r}), \psi_{\sigma'}^{\dagger}(\mathbf{r}')] = \delta_{\sigma\sigma'} \delta^3(\mathbf{r} - \mathbf{r}')$, the chemical potential is written as μ , the interaction of inter-species and intra-species are written as $g_{\uparrow\downarrow}$ and g , $\hat{R} = \lambda(\hat{p}_x - i\hat{p}_y)$ illustrates the in-plane spin-orbit-coupling, the strength of this Rashba type in-plane spin-orbit-coupling is written as λ . For convenience, we use the Rydberg atomic units that $2m = \hbar = k_B = 1$. Write the condensate density as n_0 , the basic scale of energy is set as gn_0 , thus $\sqrt{gn_0}$ is the corresponding basic scale of momentum.

Due to the translational invariance, this Hamiltonian has significant properties. In the case of non-interacting system, there are huge degenerate states of the lowest energy, that locate at the Rashba ring described by $q_x^2 + q_y^2 = (\lambda/2)^2$. When the interactions exist, this system might favor a striped phase or plane wave phase, depending on whether $g < g_{\uparrow\downarrow}$ or $g > g_{\uparrow\downarrow}$. The stripe phase is characterized by translational invariance's spontaneously being broken and the linear combinations of plane wave pairs with momenta of opposite directions, while the phase of plane wave involves just a single momentum of condensation. In general, the continuous symmetry's spontaneously being broken is expected to be the origin of the new mode of gapless Goldstone type. It is assumed that the direction of the momentum of the condensation is parallel with the axis x that $\mathbf{K} = K\hat{x}$. The form of the wave function of the condensate is represented as $\phi_{0\sigma}(\mathbf{r}) = \sum_{\alpha} \phi_{0\alpha\sigma} e^{i(2\alpha-1)\mathbf{K}\cdot\mathbf{r}}$, where σ is pseudo-spin and there is integer value of α .

Consider the parameters of variation $\phi_{0\alpha\sigma}$ and the constraint condition of K that the value of the density of total particle number is fixed at n_0 , the energy of ground state can be minimized, then the mean-field construct of the wave function of condensate is obtained, including the terms of opposite signs of phase $e^{\pm iKx}$, $e^{\pm i3Kx}$, ... corresponding to the modulation of density. The long range order of diagonal is expected to be exit by the periodic modulation shown by the density distribution.

Based on the top of the ground state of the mean-field, quantum fluctuation is considered. By the means of functional integral, this problem is treated systematically. The system's partial function is represented as

$\mathcal{Z} = \int d[\psi_\sigma^\dagger, \psi_\sigma] e^{-S}$, where the action S is described as $S = \int_0^{1/T} d\tau \int d^3\mathbf{r} \sum_\sigma \psi_\sigma^\dagger \partial_\tau \psi_\sigma + H(\psi_\sigma^\dagger, \psi_\sigma)$ [53], temperature is written as T . Using the theory of Bogoliubov, the Bose field ψ_σ is written as the summation of fluctuating part ϕ_σ and mean-field part $\phi_{0\sigma}$, illustrated by $\psi_\sigma = \phi_\sigma + \phi_{0\sigma}$. The effective action is represented as $S_{\text{eff}} = S_0 + S_g = \int d\tau d^3\mathbf{r} (\mathcal{L}_0 + \mathcal{L}_g)$, where the mean field action and the Gaussian action are written as S_0 and S_g , the mean field Lagrangian and the Gaussian Lagrangian are written as \mathcal{L}_0 and \mathcal{L}_g . The expressions of \mathcal{L}_0 and \mathcal{L}_g can be written as:

$$\mathcal{L}_0 = \sum_\sigma [\phi_{0\sigma}^* (-\nabla^2 - \mu) \phi_{0\sigma} + gn_{0\sigma}^2] + 2g_{\uparrow\downarrow} n_{0\uparrow} n_{0\downarrow} + (\phi_{0\uparrow}^* \hat{R} \phi_{0\downarrow} + c.c.) \quad (12a)$$

$$\mathcal{L}_g = \sum_\sigma [\phi_\sigma^\dagger (\partial_\tau + \hat{\xi}_\sigma) \phi_\sigma + g (\phi_{0\sigma}^2 \phi_\sigma^{\dagger 2} + h.c.)] + (\phi_{\uparrow}^* \hat{R} \phi_{\downarrow} + h.c.) + 2g_{\uparrow\downarrow} [(\phi_{0\uparrow}^* \phi_{0\downarrow}^* \phi_{\uparrow} \phi_{\downarrow} + \phi_{0\uparrow}^* \phi_{0\downarrow} \phi_{\uparrow} \phi_{\downarrow}^\dagger) + h.c.] \quad (12b)$$

where $\hat{\xi}_\sigma = -\nabla^2 - \mu + 4gn_{0\sigma} + 2g_{\uparrow\downarrow} n_{0\bar{\sigma}}$ and $n_{0\sigma} = \phi_{0\sigma}^* \phi_{0\sigma}$ are used for simplification. As well as the solution of mean-field that $\phi_{0\sigma}(\mathbf{r})$, the fluctuation fields $\hat{\phi}_\sigma(\mathbf{r})$ are expanded as:

$$\begin{pmatrix} \phi_{\uparrow}(\mathbf{r}) \\ \phi_{\downarrow}(\mathbf{r}) \end{pmatrix} = \sum_{\mathbf{q}\alpha} \begin{pmatrix} \phi_{\mathbf{q}\alpha\uparrow} \\ \phi_{\mathbf{q}\alpha\downarrow} \end{pmatrix} e^{i(2\alpha-1)\mathbf{K}\cdot\mathbf{r}} e^{i\mathbf{q}\cdot\mathbf{r}} \quad (13)$$

using this expression, we can represent S_g as:

$$\begin{aligned} S_g = & \sum_{\mathbf{q}\alpha\sigma} \phi_{\mathbf{q}\alpha\sigma}^\dagger [-iw_n + \mathbf{q}_\alpha^2 - \mu] \phi_{\mathbf{q}\alpha\sigma} \\ & + \sum_{\mathbf{q}\alpha} (R_{\mathbf{q}\alpha} \phi_{\mathbf{q}\alpha\uparrow}^\dagger \phi_{\mathbf{q}\alpha\downarrow} + h.c.) \\ & + \sum_{\mathbf{q}\alpha\beta\sigma} \left[\phi_{\mathbf{q}\alpha\sigma}^\dagger \phi_{\mathbf{q}\beta\sigma} \sum_{\alpha_1+\alpha=\alpha_2+\beta} \right. \\ & \times (4g\phi_{0\alpha_1\sigma}^* \phi_{0\alpha_2\sigma} 2g_{\uparrow\downarrow} \phi_{0\alpha_1\bar{\sigma}}^* \phi_{0\alpha_2\bar{\sigma}}) \\ & \left. + g \sum_{\alpha_1+\alpha_2=\alpha+\beta} (\phi_{0\alpha_1\sigma} \phi_{0\alpha_2\sigma} \phi_{\mathbf{q}\alpha\sigma}^\dagger \phi_{-\mathbf{q}\beta\sigma}^\dagger + h.c.) \right] \\ & + \sum_{\mathbf{q}\alpha\beta} 2g_{\uparrow\downarrow} \left[\sum_{\alpha_1+\alpha_2=\alpha+\beta} (\phi_{0\alpha_1\uparrow}^* \phi_{0\alpha_2\downarrow}^* \phi_{\mathbf{q}\alpha\uparrow} \phi_{-\mathbf{q}\beta\downarrow} + h.c.) \right. \\ & \left. + \sum_{\alpha_1+\alpha=\alpha_2+\beta} (\phi_{0\alpha_1\downarrow}^* \phi_{0\alpha_2\uparrow} \phi_{\mathbf{q}\alpha\uparrow}^\dagger \phi_{\mathbf{q}\beta\downarrow} + h.c.) \right]. \quad (14) \end{aligned}$$

It is defined that $R_{\mathbf{q}} = \lambda(q_x - iq_y)$ and $\mathbf{q}_\alpha = \mathbf{q} + (2\alpha - 1)\mathbf{K}$. In order to express the Gaussian action concisely, the column vector is defined as $\Phi_{\mathbf{q}} = (\prod_\alpha \phi_{\mathbf{q}\alpha\uparrow} \phi_{\mathbf{q}\alpha\downarrow} \prod_\beta \phi_{-\mathbf{q}\beta\uparrow}^\dagger \phi_{-\mathbf{q}\beta\downarrow}^\dagger)^T$, where α and β are integers and grouped in order of ascending. Then we can write the Gaussian action as $S_g = \frac{1}{2} \sum_{(\mathbf{q}, iw_n)} \Phi_{\mathbf{q}}^\dagger \mathcal{G}^{-1} \Phi_{\mathbf{q}} -$

$\sum_{\mathbf{q}\alpha} \frac{\xi_{\mathbf{q}\alpha}}{2}$, where the bosonic Matsubara frequencies are described as $w_n, \xi_{\mathbf{q}\alpha} = [\mathbf{q} + (2\alpha - 1)\mathbf{K}]^2 + (2g + g_{\uparrow\downarrow}) n_0 - \mu$. We can also construct the matrix elements of $\mathcal{G}_{\alpha\sigma; \alpha'\sigma'}^{-1}(\mathbf{q}, iw_n)$, the inverse Green's function conveniently from the equation above.

By the means of solving the secular function of the inverse Green's function that $\det \mathcal{G}^{-1}(\mathbf{q}, iw_n) = 0$, the excitation spectrum of the system can be found. In the case of plane wave phase [54,55], the excitation has been calculated, without the consideration of the spinor of the system, there is only one gapless branch. Consider the propagating of excitation in three dimension Cartesian coordinate system with the coordinates x, y and z , name the corresponding wave vectors as q_x, q_y and q_z . The excitation spectrum's four branches are shown. The appearance of the double gapless bands makes the stripe phase different from the uniform phases, due to the spontaneous breaking of the $U(1)$ gauge symmetry and the translational invariance symmetry. The period configuration in the space of momentum is shown by the excitation along the axis x . The behavior like free particle that $\omega_1(0, \delta q_y, 0) \propto (\delta q_y)^2$ along the axis y is shown by the lowest branch, while the behavior like phonon that $\omega_1(0, 0, \delta q_z) \propto \delta q_z$ is shown that along the axis z .

To find out the gapless band corresponding to the translational invariance symmetry breaking, we focus on the velocity of sound. In the case that the two gapless bands are limited with the limitation of long wave, the velocities of sound along the axis x are presented. When the value of interaction parameter $g_{\uparrow\downarrow}/g$ decreases, the value of the lower sound velocity V_{S1} decreases as a result, finally vanishes at $g_{\uparrow\downarrow}^c/g = 1$ which named as transition point. Then it is indicated that the V_{S1} is relative with the Goldstone mode with the spontaneous breakdown of continuous translational symmetry. When the value of interaction parameter crosses the transition point, the variation of higher velocity V_{S2} is continuous. We consider this as the sound velocity of conventional superfluid due to the breakdown of $U(1)$ gauge symmetry.

We have shown the sound velocities' two branches' directional dependence. It is obviously that both of the two branches of sound velocities have the mirror symmetry that $V_S(\theta, \varphi) = V_S(\theta, \pi + \varphi) = V_S(\pi - \theta, \varphi)$. It should be noted that the lower branch sound velocity V_{S1} vanished along the axis y , while the higher branch sound velocity V_{S2} always has finite value along all the directions. Along the directions of axis x and axis z , the velocities of sound are slight different, that shows the Rashba spin-orbit-coupling inducing anisotropy.

In this system, the thermodynamic potential can be written as $\Omega = -T \ln \mathcal{Z} = \Omega_0 + \Omega_g = TS_0 + \frac{T}{2} Tr \ln \mathcal{G}^{-1} - \frac{1}{2} \sum_{\mathbf{q}\alpha} \xi_{\mathbf{q}\alpha}$. Because of the assurance of the non-divergent behaviors, we should renormalize the interactional parameters $g_{\uparrow\downarrow}$ and g [56,57]. The correction of quantum fluctuation to the energy of ground state that $\Delta E_G = \Omega_g$ is presented. As the strength of inter-species $g_{\uparrow\downarrow}$ turned across the strength of intra-species g , the sign of the correction ΔE_G is reversed. In the case of stripe phase, ΔE_G increases when $g_{\uparrow\downarrow}$ increases, while in the case of plane wave phase, ΔE_G increases when $g_{\uparrow\downarrow}$ decreases. It

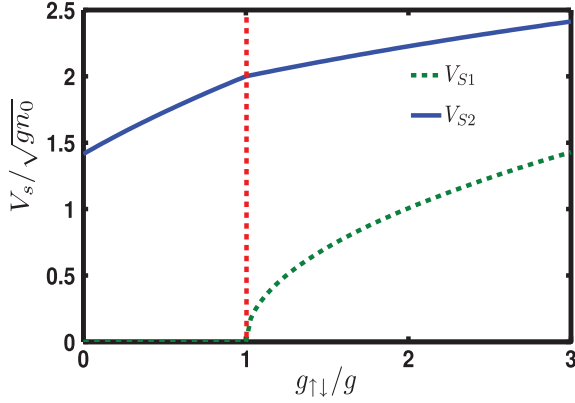


Fig. 6. The velocities of sound V_{S1} and V_{S2} along the axis x for the two lowest excitation branches as a function of interaction parameter written as $g_{\uparrow\downarrow}/g$. V_{S1} appears from the point that translational invariance is broken, and vanishes at the point of transition that $g_{\uparrow\downarrow}^c = g$ (red vertical dash line) where the phase of supersolid gives away to the phase of plane wave. V_{S2} represents the conventional sound mode corresponding to spontaneous breakdown of internal gauge symmetry. The parameter has the value that: $\lambda/\sqrt{gn_0} = 4$. This figure is taken from reference [3].

is indicated that there is a first order phase transition by the discontinuity of the ground state energy shifting. The ground state energy correction is enhanced by the spin-orbit-coupling. At the point of phase transition, it is obvious that energy correction is lower, so the phase of plane wave is preferred than the stripe phase. This is a verification of the mechanism of “order from disorder” [3] (Fig. 6).

The type of breaking symmetry in this system has fundamental effects. The discrete type symmetry leads to robust states which corresponding to gapped excitations, while the continuous type states results in infinite degenerate ground states which can evolve from each other without the cost of energy, then this system is susceptible to the effects of quantum fluctuation. In the case of Rashba type spin-orbit-coupled Bose gases, the increasing of density of states of low energy will enhance the quantum fluctuation significantly [55,58]. To make the system stable, a finite quantum depletion is required. The quantum fluctuation excited particle density is evaluated by Green’s function as: $n_{\text{ex}} = \sum_{(\mathbf{q}, i\omega_n)} \sum_{\alpha\sigma} \mathcal{G}_{\alpha\sigma, \alpha\sigma}(\mathbf{q}, i\omega_n)$. Analysis of the excitation spectrum low energy asymptotic behavior shows absence of the infra-divergence that result in a finite value of n_{ex} . The quantum depletion is enhanced by the spin-orbit-coupling and the interspecies coupling. n_{ex} is discontinuous at the point of transition that $g_{\uparrow\downarrow} = g$, characterized by the phase transition of first-order.

Compared with the case of zero-temperature, spin-orbit-coupling induced low energy state density increase will change this system in the case of finite temperature [59,60]. To extend the celebrated Bogoliubov theory from the case of zero-temperature to the case of finite temperature, we need to consider the effects of the interactions of the excitations. In this section, using the theory of Popov approximation [61], in the condition of finite

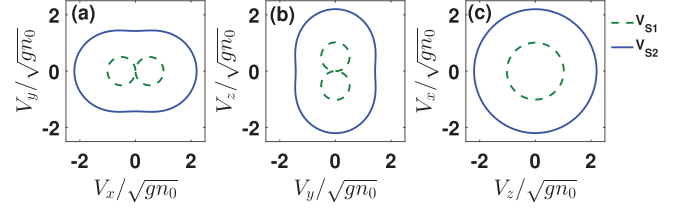


Fig. 7. The sound velocities V_{S1} and V_{S2} that have the dependence of the direction: (a) in the plane x - y ; (b) in the plane y - z ; and (c) in the plane z - x . It should be noted that the velocity of sound of the lower branch written as V_{S1} vanishes along axis y . The parameters have the values that: $\lambda/\sqrt{gn_0} = 2$ and $g_{\uparrow\downarrow}/g = 2$. These figures are taken from reference [3].

temperature, we can get a gapless spectrum and a suitable description of Bose gases. Neglecting the anomalous averages, the terms of fluctuating fields are written as [57]: $\phi_\sigma^\dagger \phi_\sigma \phi_\sigma \approx 2\langle \phi_\sigma^\dagger \phi_\sigma \rangle \phi_\sigma$, $(\phi_\sigma^\dagger \phi_\sigma)^2 \approx 4\langle \phi_\sigma^\dagger \phi_\sigma \rangle \phi_\sigma^\dagger \phi_\sigma$ and $\phi_\uparrow^\dagger \phi_\uparrow \phi_\downarrow^\dagger \phi_\downarrow \approx \langle \phi_\uparrow^\dagger \phi_\uparrow \rangle \phi_\downarrow^\dagger \phi_\downarrow + \langle \phi_\downarrow^\dagger \phi_\downarrow \rangle \phi_\uparrow^\dagger \phi_\uparrow$. Let the linear term of fluctuating fields disappear, the chemical potential shift can be written as: $\mu(T) = \mu(0) + (2g + g_{\uparrow\downarrow})n_{\text{ex}}$, where the density that excited out of condensates are written as: $n_{\text{ex}} = \sum_{\sigma} \langle \phi_\sigma^\dagger \phi_\sigma \rangle$. The Gaussian action here has a similar structure as before, except the temperature dependent n_0 (Fig. 7).

In this section, it is reviewed that supersolid phase exists in the system of Rashba type spin-orbit-coupled ultra-cold atomic condensates. This distribution of density presents a periodic modulation with the breakdown of translational symmetry that can spontaneously chose the spatial period. The elementary excitation propagates along the orientation that perpendicular to the double gapless bands featured by the stripe. The correction of quantum fluctuation to the energy of ground state presents that the discontinuous phase transition point is a first order transition point. The quantum depletion of the condensate is enhanced by the spin-orbit-coupling and the interspecies coupling. Using the method of Bragg spectroscopy [62], the sound velocity and the excitation spectrum can be probed.

5 Optical Bragg scattering of cold atoms in two-dimensional optical lattices

Quantum manipulation and quantum simulation of quantum phase can be studied on the system of ultra-cold atoms in optical lattices. Nevertheless, it is difficult to detect these quantum phases. In order to detect quantum phases, optical Bragg scattering of ultra-cold atoms loaded on optical lattices can be used, including traditional Mott insulating and superfluid phases, many kinds of charge density wave (CDW) and valence bond solid (VBS), charge density wave supersolid (CDW-SS) and valence bond supersolid (VB-SS) [4].

The ultra-cold interacting bosonic atoms loaded on optical lattices are studied by a theory of optical Bragg scattering. In this system, the optical Bragg scattering couples

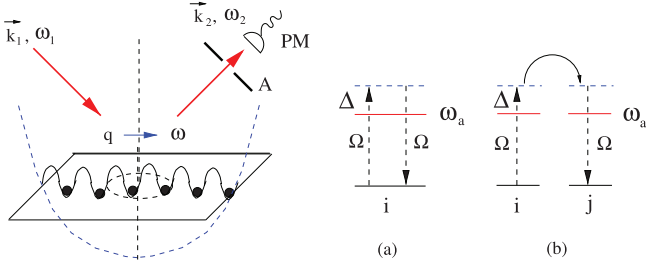


Fig. 8. The optical Bragg scattering of ultra-cold atoms in the system of two-dimensional optical lattices. The transfer energy and transfer momentum are written as $\omega = \omega_1 - \omega_2$ and $\mathbf{q} = \mathbf{k}_1 - \mathbf{k}_2$, respectively. The *Aperture* is represented as A, and the *PhotoMultiplier* is represented as PM. (a) and (b) shows the on-site term and the off-site term induced by the off-resonant scattering processes, respectively. These figures are taken from reference [4].

to the valence bond order parameter induced by the hopping of the bosonic atoms on lattices, as well as the density order parameter (Fig. 8).

In the system of two-dimensional optical lattices, the Hamiltonian of the extended Bose–Hubbard model is represented as:

$$H_{\text{BH}} = -t \sum_{\langle i,j \rangle} (b_i^\dagger b_j + H.c.) - \mu \sum_i n_i (n_i - 1) + V_i \sum_{\langle i,j \rangle} n_i n_j + V_2 \sum_{\langle i,k \rangle} n_i n_k + \dots \quad (15)$$

where the boson density is described by $n_i = b_i^\dagger b_i$; the nearest neighbor hopping is described by t , tuned by the optical lattice potential depth; the onsite interaction, the nearest neighbor interaction and the next nearest neighbor interaction are described by U , V_1 and V_2 , respectively; the possible ring-exchange interactions and further neighbor interactions are described by the ellipsis symbol. The filling factor is described by $n = N_a/N$, where atoms' number is described by N_a , lattice sites' number is described by N . The Feshbach resonance can be used to tune the onsite interaction U [63]. Many types of optical lattices can be realized by constructing the suitable optical lattices with the suitable geometry of laser beams, such as Kagome, body-centered-cubic, triangular and honeycomb lattices [64,65]. In the optical lattices, long range interaction interactions of the ultra-cold atoms can be constructed in many ways. In the system of the two-dimensional optical lattice loading Chromium-52 atoms [66] or polar molecules [67] with dipole moments vertical to the trapping plane is represented by extended boson Hubbard model with p^3/r_2 which described the long range repulsive interaction, where the dipole moment is described by p . By the numerical simulation, the CDW-SS could be found stable in this system within a large regime of parameter.

The Hamiltonian of the interaction between the two laser beams with two level ultra-cold bosonic atoms is

written as:

$$H_{\text{int}} = \int d^2\mathbf{r} \Psi^\dagger(\mathbf{r}) \left[\frac{\mathbf{p}^2}{2m_a} + V_{\text{OL}}(\mathbf{r}) + \frac{\hbar\omega_a}{2} \sigma_z + \frac{\Omega}{2} \sum_l (e^{-i\omega_l t} \sigma^+ u_l(\mathbf{r}) + h.c.) \right] \Psi(\mathbf{r}) \quad (16)$$

where the operator of two component boson annihilation is represented as $\Psi(\mathbf{r}) = (\psi_e, \psi_g)$, frequencies ω_l are the frequencies of the incident and scattered lights, $u_l(\mathbf{r}) = e^{i\mathbf{k}_l \cdot \mathbf{r} + i\phi_l}$ are the mode functions. In this system, Rabi frequencies Ω are very weak when compared with the laser beams that constructing the optical lattices. The difference of the two energy level is ω_a , then the detunings of laser atoms are $\Delta_l = \omega_l - \omega_a$, when it is far away from the resonance. Difference of the energy level is much larger than the energy transfer $\omega = \omega_1 - \omega_2$ and the Rabi frequency Ω , then we can make an approximate that $\Delta_1 \sim \Delta_2 = \Delta$. Let the upper energy level e be eliminated adiabatically, expanding the field operator of the ground state atom as $\psi_g(\mathbf{r}) = \sum_i b_i w(\mathbf{r} - \mathbf{r}_i)$, where the Wannier functions of the $V_{\text{OL}}(\mathbf{r})$ corresponding to lowest Bloch band are represented as $w(\mathbf{r} - \mathbf{r}_i)$, the atom's annihilation operator on the site i is represented as b_i . Then the Hamiltonian of the effective interaction between the ground state g and the off-resonant laser beams is represented as:

$$H_{\text{int}} = \hbar \frac{\Omega^2}{\Delta} e^{-i\omega t} \left[\sum_i J_{i,i} n_i + \sum_{\langle i,j \rangle} J_{i,j} b_i^\dagger b_j \right] \quad (17)$$

where $J_{i,j} = \int d\mathbf{r} w(\mathbf{r} - \mathbf{r}_i) u_1^*(\mathbf{r}) u_2(\mathbf{r}) w(\mathbf{r} - \mathbf{r}_j) = J_{j,i}$ represents the matrix element of interaction, $\sum_i J_{i,i} n_i$ represents the on-site interaction and we can define that $\hat{D} = \sum_i J_{i,i} n_i$, $\sum_{\langle i,j \rangle} J_{i,j} b_i^\dagger b_j$ represents the off-site interaction and we can define that $\hat{K} = \sum_{\langle i,j \rangle} J_{i,j} b_i^\dagger b_j$. In the lowest Bloch band, Wannier function can be considered as real function, so we represent off-site interaction as $\hat{K} = \sum_{\langle i,j \rangle} J_{i,j} (b_i^\dagger b_j + h.c.)$, $b_i^\dagger b_j + h.c.$ is the off-site coupling to the Bose atoms' nearest neighbor kinetic energy, we can define that $K_{ij} = b_i^\dagger b_j + h.c.$

It is obvious that:

$$\hat{D}(\mathbf{q}) = f_0(\mathbf{q}) \sum_{i=1}^N e^{-i\mathbf{q} \cdot \mathbf{r}_i} n_i = N f_0(\mathbf{q}) n(\mathbf{q}) \quad (18)$$

where $f_0(\mathbf{q}) = \int d\mathbf{r} e^{-i\mathbf{q} \cdot \mathbf{r}} w^2(\mathbf{r})$, $\mathbf{q} = \mathbf{k}_1 - \mathbf{k}_2$, and the density operator's Fourier transformation at the momentum \mathbf{q} represented as $n(\mathbf{q}) = \frac{1}{N} \sum_{i=1}^N e^{-i\mathbf{q} \cdot \mathbf{r}_i} n_i = \sum_{\mathbf{k}} b_{\mathbf{k}}^\dagger b_{\mathbf{k}+\mathbf{q}}$. It should be noted that $n(\mathbf{q}) = n(\mathbf{q} + \mathbf{K})$, where the reciprocal lattice vector is represented as \mathbf{K} . The wave vector q is confined in an interval that $L^{-1} < q < a^{-1}$, where $L \sim 100 \mu\text{m}$ represents the trap size and $a \sim 0.5 \mu\text{m}$ represents the lattice constant. Actually, the off-site kinetic coupling contains much more interesting information. In the optical lattice of square structure, since the orientation of the bonds can only forward the same of the \hat{x} axis

or the \hat{y} axis, we can represent the bonds as:

$$\hat{K}_{\text{square}} = N [f_x(\mathbf{q}) K_x(\mathbf{q}) + f_y(\mathbf{q}) K_y(\mathbf{q})] \quad (19)$$

where the function $f_\alpha(\mathbf{q}) = f(\mathbf{q}, \mathbf{r}_i - \mathbf{r}_j = \alpha) = \int d\mathbf{r} e^{-i\mathbf{q}\cdot\mathbf{r}} w(\mathbf{r}) w(\mathbf{r} + \mathbf{r}_i - \mathbf{r}_j)$, $\alpha = x, y$ represents the form factors and the Fourier transformations of the operator of kinetic energy $K_{ij} = b_i^\dagger b_j + h.c.$ that forwards the same direction of $\alpha = x, y$ bonds with the momentum \mathbf{q} represented as $K_\alpha(\mathbf{q}) = \frac{1}{N} \sum_{i=1}^N e^{-i\mathbf{q}\cdot\mathbf{r}_i} K_{i,i+\alpha} = e^{i\mathbf{q}\cdot\alpha/2} \sum_{\mathbf{k}} \cos k_\alpha b_{\mathbf{k}}^\dagger b_{\mathbf{k}+\mathbf{q}}$, $\alpha = x, y$. It is similar as $n(\mathbf{q}) = n(\mathbf{q} + \mathbf{K})$ that $K_\alpha(\mathbf{q}) = K_\alpha(\mathbf{q} + \mathbf{K})$. Evaluation of harmonic approximation [63] shows that $f_x(\pi, 0) \sim i e^{-\frac{1}{4}(V_0/E_r)^{-1/2} - \frac{\pi^2}{4}(V_0/E_r)^{1/2}}$ and $f_0(\pi, 0) \sim e^{-\frac{1}{4}(V_0/E_r)^{-1/2}}$, then $|f_x(\pi, 0)/f_0(\pi, 0)| \sim e^{-\frac{\pi^2}{4}\sqrt{V_0/E_r}}$, where the potential of optical lattice and the energy of the recoil are represented as V_0 and $E_r = \hbar^2 k^2/2m$. When $V_0/E_r > 4$, the value of $f_0(\pi, 0)$ is close to 1. Compare this ratio with the ratio of the hopping t of the on-site interaction U : $|f_x(\pi, 0)/f_0(\pi, 0)| \sim \frac{t}{U} \frac{a_s}{a}$, where the scattering length of zero field is represented as a_s and the optical lattice constant is represented as $a = \lambda/2 = \pi/k$. Choosing the characteristic values that $t/U \sim 10^{-1}$, $a_s/a \sim 10^{-2}$, we can evaluate that $|f_\alpha/f_0| \sim 10^{-3}$. It should be noted that only in the system of optical lattice that $V_0 \gg E_r$, the harmonic approximation can be effective, so the value calculated above must be underestimated, in fact, it is expected that $|f_\alpha/f_0| \geq 10^{-3}$.

By the theory of standard linear response, the differential cross section of the photons that scattered from the system of cold atoms can be described:

$$\frac{d\sigma}{d\Omega dE} = S(\mathbf{q}, \omega) \sim \left(\frac{\Omega^2}{\Delta}\right)^2 N^2 \left[|f_0(\mathbf{q})|^2 S_n(\mathbf{q}, \omega) + \sum_{\alpha=\hat{x}, \hat{y}} |f_\alpha(\mathbf{q})|^2 S_{K_\alpha}(\mathbf{q}, \omega) \right] \quad (20)$$

in this equation, $\omega = \omega_1 - \omega_2$, $\mathbf{q} = \mathbf{k}_1 - \mathbf{k}_0$, and the function of dynamic density-density response is represented by $S_n(\mathbf{q}, \omega) = \langle n(-\mathbf{q}, -\omega) n(\mathbf{q}, \omega) \rangle$. The function of bond-bond response is represented as $S_{K_\alpha}(\mathbf{q}, \omega) = \langle K_\alpha(-\mathbf{q}, -\omega) K_\alpha(\mathbf{q}, \omega) \rangle$.

The transition from superfluid state to Mott state can be analyzed with the integer filling factor n . Let the \mathbf{q} equal to $\mathbf{K} = (2\pi, 0)$ which describes the shortest reciprocal lattice vector. In superfluid state, we have $\frac{d\sigma^{\text{SF}}}{d\Omega} \sim |f_0^{\text{SF}}(2\pi, 0)|^2 N^2 n^2 + 2|f_x^{\text{SF}}(2\pi, 0)|^2 N^2 B^2$, where the average kinetic energy of a bond in superfluid side is represented as B . In the case of Mott state, we have $\frac{d\sigma^{\text{M}}}{d\Omega} \sim |f_0^{\text{M}}(2\pi, 0)|^2 N^2 n^2$. Because the average kinetic energy B is detectable in the superfluid side only and approximate evaluation shows that $|f_0^{\text{SF}}(2\pi, 0)|^2 \sim |f_0^{\text{M}}(2\pi, 0)|^2 \sim 1$, the increasing of scattering cross section due to the pre-factor N^2 that across from Mott state to the superfluid state can be expected as:

$$\frac{d\sigma^{\text{SF}}}{d\Omega} - \frac{d\sigma^{\text{M}}}{d\Omega} = 2|f_x^{\text{SF}}(2\pi, 0)|^2 N^2 B^2 \quad (21)$$

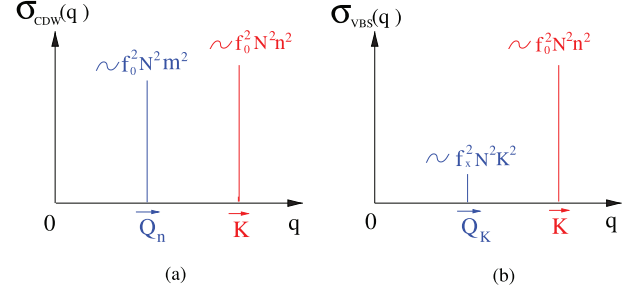


Fig. 9. The cross section of optical scattering in (a) CDW, where the ratio of the peaks at \mathbf{Q}_n over \mathbf{K} is approximated as $m^2/n^2 \sim 1$. The cross section of optical scattering in (b) VBS state, where the ratio of the peaks at \mathbf{Q}_K over \mathbf{K} is approximated as $|f_x/f_0|^2 K^2/n^2 \geq 10^{-5}$, which in the experiments of current optical Bragg scattering still visible. These figures are taken from reference [4].

because of the lack of the VBS order in CDW when $\mathbf{Q}_n = (\pi, \pi)$, the second term in equation (6) is too small that can be ignored, so we have:

$$\frac{d\sigma}{d\Omega dE} |_{\text{CDW}} \sim \left(\frac{\Omega^2}{\Delta}\right)^2 N^2 |f_0(\mathbf{q})|^2 S_n(\mathbf{q}, \omega) \quad (22)$$

it should be showed that there is a peak when $\mathbf{q} = \mathbf{Q}_n$, that the square of the atoms' number in trap is the scale of amplitude $\sim |f_0(\pi, \pi)|^2 N^2 m^2$, where the order parameter of the CDW is described as $m = n_A - n_B$ [68]. Let $\mathbf{q} = \mathbf{K}$, so that $S_{\text{CDW}}(\mathbf{K}) \sim |f_0(2\pi, 0)|^2 N^2 n^2$, there is a relation that $f_0(2\pi, 0) \sim f_0^2(\pi, \pi)$. If we ignore the little difference between the two form factors, the ratio of these two peaks could be estimated as $\sim m^2/n^2$. Through a second order phase transition [68], CDW might transit into CDW-SS, when the filling is slightly away from $1/2$. Define that $n = n_A + n_B = 1/2 + \delta n$, we can get $\langle n(\mathbf{q}) \rangle = m\delta_{\mathbf{q}, \mathbf{Q}_n} + n\delta_{\mathbf{q}, 0}$. The density of the superfluid can be written as $\rho_s \sim \delta n = n - 1/2$. The scattering cross section in the CDW-SS is similar like the scattering cross section in the CDW: $S_{\text{CDW-SS}}(\mathbf{Q}_n) \sim |f_0(\pi, \pi)|^2 N^2 m^2$, while $S_{\text{CDW-SS}}(\mathbf{K}) \sim |f_0(2\pi, 0)|^2 N^2 n^2 + 2|f_x(2\pi, 0)|^2 N^2 (\delta n)^2 B^2$ will be increased. The strength of average bond B induced by the small component of superfluid $\rho_s \sim \delta n = n - 1/2$ that flowing through the lattice entirely. Because of the component of the superfluid in the CDW-SS phase and the increasing of the total density, the right peak will be increased (Fig. 9).

Compared to the CDW state, the VBS state will be discussed when $\mathbf{Q}_K = (\pi, 0)$. In VBS, there is a uniform density distribution, if $\mathbf{q} = \mathbf{K}$, the differential cross equation could be simplified that the second term of equation (6) could be ignored, then we have the diffraction peak with the scale of amplitude described by the square of atoms' number in the trap that $\sim |f_0(2\pi, 0)|^2 N^2 n^2$, where the VBS state's uniform density described as $n = 1/2$ and $f_0(2\pi, 0) \sim f_0^4(\pi, 0)$. Nevertheless, if the \mathbf{q} is near the \mathbf{Q}_K , we could ignore the first term of differential scattering

cross section, then we have:

$$\frac{d\sigma}{d\Omega dE}|_{\text{VBS}} \sim \left(\frac{\Omega^2}{\Delta}\right)^2 N^2 \sum_{\alpha=\hat{x},\hat{y}} |f_\alpha(\mathbf{q})|^2 S_{K_\alpha}(\mathbf{q}, \omega) \quad (23)$$

this equation shows that there is a peak at $\mathbf{q} = \mathbf{Q}_K$ that characterizes the VBS ordering, and the scale of amplitude described by the square of the atoms' number in the trap $\sim |f_x(\pi, 0)|^2 N^2 K^2$, where the order parameter is represented as $K = K_x - K_y$ [68]. Then we have the relation that $K^2/n^2 |f_x(\pi, 0)/f_0(2\pi, 0)|^2 \geq 10^{-5}$. When the filling is slightly away from 1/2, through a second order phase transition [68], VBS is turned into VB-SS. Because of the superfluid component in VB-SS phase and the increasing of the total density, right peak will be increased. When $\mathbf{q} = \mathbf{Q}_K = (0, \pi)$, the VBS order can be discussed similarly. The $S_K(\mathbf{q})$ peaks at $(\pi, 0)$ and $(0, \pi)$ should be observed because of the existence of the order of plaquette VBS. By the method of Bragg scattering, we can distinguish the plaquette VBS and the dimer VBS.

In this section, to detect various ground states with the system of square lattice, the method of optical Bragg scattering is reviewed.

6 Summary

In this article, several important cases about the supersolid have been reviewed. The coexistence of the diagonal long-range order of solid and the off-diagonal long-range order of superfluid characterizes the supersolid phase. To investigate supersolid phase, we discussed several circumstances of cold atoms, such as cold atoms with spin-orbit-coupling in spin dependent periodic potential with hard-core or soft-core long-range interactions, three-dimensional cold atoms with spin-orbit-coupling of Rashba type and optical Bragg scattering in optical lattices. The combination of the spin-orbit-coupled ultracold hard-core atoms with contact interaction and the spin-dependent potential can be used to build supersolid phase. The interplay of spin-orbit-coupling and soft-core long-range interaction can construct exotic supersolid phase, which contains the spontaneous breakdown of the symmetry of chirality. The optical Bragg scattering can be used to detect the supersolid phase in the system of ultracold atoms in optical lattices. Investigation of supersolid phase can make progress to go beyond the existing knowledge about the separation of phase and the generating of angular momentum.

As a phase of matter, supersolid phases have been theoretically predicted many years ago [13]. With the development of modern physics in theories and experimental instruments, scientists have made great progress about the investigating of matter phases including the supersolid phase. Supersolid can be understood as the combination of diagonal and off-diagonal long-range orders of both solids and superfluids [1,2]. The system of cold atoms in optical lattice has supported a good platform for the investigation of supersolid. In recent years, scientists have observed the supersolid phase experimentally [69,70].

This article has reviewed some of the recent developments about the investigation of supersolids. We expect that the combination of the theoretic analysis and experimental realization of the novel physics of supersolid phenomena can be heuristic for the development of modern physical researches.

This work was supported by the National Key R&D Program of China under grant no. 2016YFA0301500, NSFC under grant no. 61835013, Strategic Priority Research Program of the Chinese Academy of Sciences under grant nos. XDB01020300, XDB21030300.

Author contribution statement

Wei Han, Ren-Yuan Liao and Jin-Wu Ye provided the basic ideas and the calculation results, Tie-Fu Zhang and Wu-Ming Liu wrote this paper.

Publisher's Note The EPJ Publishers remain neutral with regard to jurisdictional claims in published maps and institutional affiliations.

References

1. W. Han, G. Juzeliūnas, W. Zhang, W.M. Liu, Phys. Rev. A **91**, 013607 (2015)
2. W. Han, X.F. Zhang, D.S. Wang, H.F. Jiang, W. Zhang, S.G. Zhang, Phys. Rev. Lett. **121**, 030404 (2018)
3. R. Liao, Phys. Rev. Lett. **120**, 140403 (2018)
4. J. Ye, J.M. Zhang, W.M. Liu, K. Zhang, Y. Li, W. Zhang, Phys. Rev. A **83**, 051604(R) (2011)
5. S. Balibar, Nature (London) **464**, 176 (2010)
6. E. Kim, M.H.W. Chan, Nature (London) **427**, 225 (2004)
7. J. Ye, Phys. Rev. Lett. **97**, 125302 (2006)
8. J. Day, J. Beamish, Nature (London) **450**, 853 (2007)
9. B. Hunt, E. Pratt, V. Gadagkar, M. Yamashita, A.V. Balatsky, J.C. Davis, Science **324**, 632 (2009)
10. H. Choi, D. Takahashi, K. Kono, E. Kim, Science **330**, 1512 (2010)
11. A.F. Andreev, I.M. Lifshitz, Sov. Phys. JETP **29**, 1107 (1969)
12. G.V. Chester, Phys. Rev. A **2**, 256 (1970)
13. A.J. Leggett, Phys. Rev. Lett. **25**, 1543 (1970)
14. M.W. Meisel, Physica B **178**, 121 (1992)
15. S. Balibar, F. Caupin, J. Phys.: Condens. Matter **20**, 173201 (2008)
16. M. Boninsegni, N.V. Prokof'ev, Rev. Mod. Phys. **84**, 759 (2012)
17. N. Henkel, R. Nath, T. Pohl, Phys. Rev. Lett. **104**, 195302 (2010)
18. F. Cinti, P. Jain, M. Boninsegni, A. Micheli, P. Zoller, G. Pupillo, Phys. Rev. Lett. **105**, 135301 (2010)
19. N. Henkel, F. Cinti, P. Jain, G. Pupillo, T. Pohl, Phys. Rev. Lett. **108**, 265301 (2012)
20. S. Wessel, M. Troyer, Phys. Rev. Lett. **95**, 127205 (2005)
21. I. Danshita, C.A.R. Sá de Melo, Phys. Rev. Lett. **103**, 225301 (2009)
22. O. Tieleman, A. Lazarides, C. Morais Smith, Phys. Rev. A **83**, 013627 (2011)

23. B.M. Anderson, I.B. Spielman, G. Juzeliūnas, Phys. Rev. Lett. **111**, 125301 (2013)
24. Z.F. Xu, L. You, M. Ueda, Phys. Rev. A **87**, 063634 (2013)
25. I.H. Deutsch, P.S. Jessen, Phys. Rev. A **57**, 1972 (1998)
26. O. Mandel, M. Greiner, A. Widera, T. Rom, T.W. Hänsch, I. Bloch, Phys. Rev. Lett. **91**, 010407 (2003)
27. C.J. Pethick, H. Smith, *Bose–Einstein Condensation in Dilute Gases* (Cambridge University Press, Cambridge, 2002)
28. G.E. Volovik, *The Universe in a Helium Droplet* (Oxford University Press, New York, 2003)
29. K. Kasamatsu, M. Tsubota, M. Ueda, Phys. Rev. Lett. **93**, 250406 (2004)
30. V. Schweikhard, I. Coddington, P. Engels, S. Tung, E.A. Cornell, Phys. Rev. Lett. **93**, 210403 (2004)
31. S.W. Su, C.H. Hsueh, I.K. Liu, T.L. Horng, Y.C. Tsai, S.C. Gou, W.M. Liu, Phys. Rev. A **84**, 023601 (2011)
32. H. Hu, B. Ramachandhran, H. Pu, X.J. Liu, Phys. Rev. Lett. **108**, 010402 (2012)
33. B.A. Malomed, H.E. Nistazakis, D.J. Frantzeskakis, P.G. Kevrekidis, Phys. Rev. A **70**, 043616 (2004)
34. G. Chen, T. Ma, A.T. N'Diaye, H. Kwon, C. Won, Y. Wu, A.K. Schmid, Nat. Commun. **4**, 2671 (2013)
35. K.S. Ryu, L. Thomas, S.H. Yang, S. Parkin, Nat. Nanotechnol. **8**, 527 (2013)
36. S. Emori, U. Bauer, S.M. Ahn, E. Martinez, G.S.D. Beach, Nat. Mater. **12**, 611 (2013)
37. P.T. Ernst, S. Götze, J.S. Krauser, K. Pyka, D.S. Lühmann, D. Pfannkuche, K. Sengstock, Nat. Phys. **6**, 56 (2010)
38. N. Gemelke, X. Zhang, C.L. Hung, C. Chin, Nature (London) **460**, 995 (2009)
39. W.S. Bakr, A. Peng, M.E. Tai, R. Ma, J. Simon, J.I. Gillen, S. Fölling, L. Pollet, M. Greiner, Science **329**, 547 (2010)
40. D. Bohm, Phys. Rev. **75**, 502 (1949)
41. Y. Ohashi, T. Momoi, J. Phys. Soc. Jpn. **65**, 3254 (1996)
42. Y.J. Lin, R.L. Compton, K. Jiménez-García, J.V. Porto, I.B. Spielman, Nature (London) **462**, 628 (2009)
43. K.W. Madison, F. Chevy, W. Wohlleben, J. Dalibard, Phys. Rev. Lett. **84**, 806 (2000)
44. J.R. Abo-Shaeer, C. Raman, J.M. Vogels, W. Ketterle, Science **292**, 476 (2001)
45. C.H. Hsueh, Y.C. Tsai, K.S. Wu, M.S. Chang, W.C. Wu, Phys. Rev. A **88**, 043646 (2013)
46. S. Sinha, R. Nath, L. Santos, Phys. Rev. Lett. **107**, 270401 (2011)
47. S.W. Su, I.K. Liu, Y.C. Tsai, W.M. Liu, S.C. Gou, Phys. Rev. A **86**, 023601 (2012)
48. Z.F. Xu, Y. Kawaguchi, L. You, M. Ueda, Phys. Rev. A **86**, 033628 (2012)
49. E. Ruokokoski, J.A.M. Huhtamäki, M. Möttönen, Phys. Rev. A **86**, 051607(R) (2012)
50. Z.F. Xu, S. Kobayashi, M. Ueda, Phys. Rev. A **88**, 013621 (2013)
51. S.W. Su, S.C. Gou, Q. Sun, L. Wen, W.M. Liu, A.C. Ji, J. Ruseckas, G. Juzeliūnas, Phys. Rev. A **93**, 053630 (2016)
52. D.S. Hall, M.R. Matthews, J.R. Ensher, C.E. Wieman, E.A. Cornell, Phys. Rev. Lett. **81**, 1539 (1998)
53. A. Altland, B. Simons, *Condensed Matter Field Theory*, 2nd edn. (Cambridge University Press, Cambridge, 2010)
54. R. Liao, Z.G. Huang, X.M. Lin, W.M. Liu, Phys. Rev. A **87**, 043605 (2013)
55. T. Ozawa, G. Baym, Phys. Rev. Lett. **109**, 025301 (2012)
56. H. Stoof, K. Gubbels, D. Dickercheid, *Ultracold Quantum Fields* (Springer, Bristol, 2009)
57. J.O. Anderson, Rev. Mod. Phys. **76**, 599 (2004)
58. Q. Zhou, X. Cui, Phys. Rev. Lett. **110**, 140407 (2013)
59. T. Ozawa, G. Baym, Phys. Rev. Lett. **110**, 085304 (2013)
60. R. Liao, Z.G. Huang, X.M. Lin, O. Fialko, Phys. Rev. A **89**, 063614 (2014)
61. V. Popov, *Functional Integrals in Quantum Field Theory and Statistical Physics* (Reidel, Dordrecht, 2001)
62. S.C. Ji, L. Zhang, X.T. Xu, Z. Wu, Y. Deng, S. Chen, J.W. Pan, Phys. Rev. Lett. **114**, 105301 (2015)
63. D. Jaksch, C. Bruder, J.I. Cirac, C.W. Gardiner, P. Zoller, Phys. Rev. Lett. **81**, 3108 (1998)
64. G. Grynberg, B. Lounis, P. Verkerk, J.Y. Courtois, C. Salomon, Phys. Rev. Lett. **70**, 2249 (1993)
65. L. Santos, M.A. Baranov, J.I. Cirac, H.-U. Everts, H. Fehrmann, M. Lewenstein, Phys. Rev. Lett. **93**, 030601 (2004)
66. A. Griesmaier, J. Werner, S. Hensler, J. Stuhler, T. Pfau, Phys. Rev. Lett. **94**, 160401 (2005)
67. K.K. Ni, S. Ospelkaus, M.H.G. de Miranda, A. Pe'er, B. Neyenhuis, J.J. Zirbel, S. Kotochigova, P.S. Julienne, D.S. Jin, J. Ye, Science **322**, 231 (2008)
68. J. Ye, Nucl. Phys. B **805**, 418 (2008)
69. J.R. Li, J. Lee, W. Huang, S. Burchesky, B. Shteynas, F.Ç. Top, A.O. Jamison, W. Ketterle, Nature (London) **543**, 91 (2017)
70. J. Léonard, A. Morales, P. Zupancic, T. Esslinger, T. Donner, Nature **543**, 87 (2017)